Journal of Hazardous Materials 459 (2023) 132166

Contents lists available at ScienceDirect

Journal of Hazardous Materials

journal homepage: www.elsevier.com/locate/jhazmat

Tracking the multiple Hg sources in sediments in a typical river-lake basin by isotope compositions and mixing models

Lulu Mao [a], Wenbo Ren [a], Xitao Liu [a,*], Mengchang He [a], Chunye Lin [a], Ying Zhong [b], Yang Tang [b], Wei Ouyang [a,c]

[a] State Key Laboratory of Water Environment Simulation, School of Environment, Beijing Normal University, Beijing 100875, China
[b] State Key Laboratory of Ore Deposit Geochemistry, Institute of Geochemistry, Chinese Academy of Sciences, 550081 Guiyang, China
[c] Advanced Interdisciplinary Institute of Environment and Ecology, Beijing Normal University, Zhuhai 519087, China

HIGHLIGHTS

- Four Hg sources were defined by varied Hg isotope signatures in the Zijiang River.
- Hg sources were industrial Hg, urban Hg, background Hg and atmospheric Hg.
- The principal Hg source in the Zijiang River was from industrial discharges.
- Non-ferrous smelting dominated Hg sources in the Lianxi River.
- MIF characteristics were attributed to incomplete process of Hg^{2+} photoreduction.

GRAPHICAL ABSTRACT

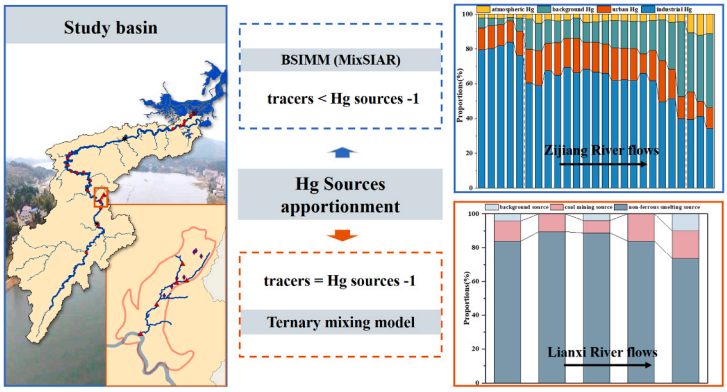

ARTICLE INFO

Editor: Edward Burton

Keywords:
Hg isotope signatures
Bayesian stable isotope mixing model
Source apportionment
Zijiang River basin

ABSTRACT

In this study, total mercury (THg) contents and Hg isotope compositions in sediments were investigated in the Lianxi River, Zijiang River and South Dongting Lake to identify and quantify multiple Hg sources and evaluate the Hg environmental processes. The THg contents, $\delta^{202}Hg$ and $\Delta^{199}Hg$ values in sediments were 48.22 ~ 4284.32 μg/kg, − 1.33 ~ 0.04‰ and − 0.25 ~ 0.03‰, respectively. Relatively distinct Hg isotope characteristics of sediments were presented in the Lianxi River, Zijiang River and South Dongting Lake, indicating the dominant Hg sources considerably varied in these regions. Source apportionment based on MixSIAR proved that Hg in sediments mainly originated from industrial activities, and the ternary mixing model concluded non-ferrous metal smelting was the dominant industrial Hg contributor in the Lianxi River. Compared with the Lianxi River, the relative contribution of Hg in sediments from industrial activities significantly decreased, while the relative contributions of Hg from background releases significantly increased in the Zijiang River and South

Abbreviations: Hg,, mercury; THg,, total mercury; MDF,, mass dependent fractionation; MIF,, mass independent fractionation; BSIMM,, Bayesian stable isotope mixing model; MixSIAR,, Mixing Stable Isotope Analysis in R; MixSIR,, Mixing Stable Isotope in R; SIAR,, Stable Isotope Analysis in R; DEM,, Digital Elevation Model; SOM,, organic matter in sediments; MGD,, mean grain diameter; MCMC,, Markov chain Monte Carlo.

* Corresponding author.
E-mail address: liuxt@bnu.edu.cn (X. Liu).

https://doi.org/10.1016/j.jhazmat.2023.132166
Received 18 April 2023; Received in revised form 25 July 2023; Accepted 26 July 2023
Available online 27 July 2023

Dongting Lake. Nonetheless, the contribution of industrial Hg in this study area deserves more attention. These results are conducive to further manage Hg pollution.

1. Introduction

Mercury (Hg), a highly toxic metal, is ubiquitously found in the aqueous and terrestrial ecosystems [1]. Hg enters the environments through natural releasing processes (e.g. rock weathering, volcanic eruptions and hydrothermal activities) [2,3] and anthropogenic discharges (e.g. mining, smelting and coal burning) [4]. Small-scale gold mining [5,6], coal combustion [7], non-ferrous smelting [8] and cement production [9] are considered as the important industrial Hg contributors. These industrial sectors release Hg by wastewater and flue gas, resulting in Hg contamination in adjacent aquatic ecosystems [10,11].

Zijiang River basin has abundant mineral resources, prosperous industries and populated cities with a total of 10 million people [12]. The released gaseous Hg by the mining and smelting activities is diffused into the atmosphere and deposited to the aquatic ecosystems [8], and the Hg-containing wastewater discharged by smelters and chemical plants is carried into the aqueous environments [5]. In addition, urban activities also might contribute to Hg pollution to adjacent environments, such as waste incineration, domestic sewage discharges and vehicle exhaust emissions [13]. The Lianxi River, the important component of the Zijiang River, flows through the Capital of Antimony (Xikuangshan), receives the industrial discharges and transports contaminants into the Zijiang River. Numerous non-ferrous metal smelting plants and coal mining and processing industries are located in the Xikuangshan [14], thus, the Lianxi River is considerably affected by multiple industrial sources.

The Hg isotope signatures provide sound evidence for quantifying the potential Hg sources and identifying the biogeochemical pathways in the ecosystems [5,15]. Hg presents seven stable isotopes in natural environment. Mass dependent fractionation (MDF) and mass independent fractionation (MIF) of Hg isotopes significantly vary in various geochemical behavior [16]. MDF (expressed by δ^{202}Hg) is widely induced in almost all physical reactions, abiotic chemical reactions and microbial-mediated reactions, such as volatilization [17], methylation [18] and chemical reduction [19]. In contrast, MIF (characterized by Δ^{199}Hg) is primarily occurred in photochemical reaction, such as photoreduction [20] and photodegradation [21]. Largely varied δ^{202}Hg and Δ^{199}Hg values were found in sediments in rivers [13,22], lakes [23, 24], seas [25,26], reservoirs [27]; Zhao et al., 2021), estuaries [26,28] and bays [29,30]. δ^{202}Hg is a vital indicator for evaluating anthropogenic Hg in sediments, rising with the increasing industrial Hg emission [11,31]. The Hg isotope compositions of δ^{202}Hg and Δ^{199}Hg in sediments have been adopted to trace the anthropogenic and natural Hg in environment [22,26]. Liu et al. [13] reported heavier δ^{202}Hg and Δ^{199}Hg values of sediments in industrial area in the Dongjiang River than those in urban area and background area. Moreover, the sediments affected by different industrial point sources showed near-zero Δ^{199}Hg values and relatively distinct δ^{202}Hg [32]. Furthermore, binary and ternary mixing models were developed to quantify the contributions of different Hg sources with distinct Hg isotope characteristics in sediments [26]. Ma et al. [33] evaluated the differences in δ^{202}Hg values of background source and anthropogenic source in three lakes near the Flin Flon smelter, and further quantify the relative contributions of Hg sources by a binary model. The varied signatures of δ^{202}Hg and Δ^{199}Hg have been reported in Chinese coastal sediments, and the relative contributions of direct discharge of industrial activities, riverine inputs and atmospheric deposition were further quantified by a triple mixing model [34].

In a mixing system with well-defined Hg isotope end-members, different source apportionment methods correspond to distinct numbers of isotope tracers and sources. Specifically, the linear mixing model is successfully used at tracers = sources − 1 [35], the least squares solution by iteration is adopted at tracers > sources − 1 [36], the Bayesian stable isotope mixing model (BSIMM) is the appropriate method at tracers < sources − 1 [37]. Mixing Stable Isotope Analysis in R (MixSIAR), the latest generation of BSIMM, incorporates the theory developments in BSIMM since Mixing Stable Isotope in R (MixSIR) and Stable Isotope Analysis in R (SIAR) [38] and improves the capability of quantifying multiple sources in mixing systems, which has been applied in quantifying Pb isotope sources [39], carbon sources [40] and nitrate sources [41].

This study sought to: 1) investigate the THg contents and Hg isotope values in sediments; 2) evaluate the signatures of MDF and MIF compositions in sediments; 3) identify and quantify the relative contributions of multiple Hg sources in sediments in the Zijiang River and 4) quantify the dominant industrial Hg source in sediments in the Lianxi River.

2. Material and methods

2.1. Field locations and sampling

Zijiang River is an important component of the Yangtze River system. The Zijiang River lies 653 km, flows through numerous cities, mining areas and industrial areas in Hunan Province from south to north and merges into the Dongting Lake (Fig. 1a). The Zijiang River basin covers 28142 km^2 and supports about 10 million residents [12]. Lianxi River is a major tributary in midstream in the Zijiang River, flows through the super large antimony mine (Xikuangshan), and injects into the Zijiang River in Lengshuijiang. Many industrial activities in the Xikuangshan distribute along the Lianxi River, including non-ferrous metal smelting plants (M1-M5) and coal mining and processing plants (M6-M7) (Fig. 1b).

Twenty-five surface sediment samples (0–20 cm) were collected with a stainless-steel grab sampler in September 2020. Three groups of sediments were classified (Fig. 1): specifically, the first group included 17 sediment samples from the Zijiang River (upstream: Z1-Z2; midstream: Z3-Z12; downstream: Z13-Z17); the second group included 5 sediment samples from the Lianxi River (L1-L5); the third group included 3 sediment samples from the South Dongting Lake (SD1-SD3). The collected sediment samples were immediately placed in clean polyethylene plastic bags, transferred to stainless steel boxes to avoid crossed-contamination and then transported to the laboratory and stored in a refrigerator at − 20 °C. Then, the sediments were dried with a freeze dryer (LGJ-10, China) at − 70 °C for 48 h, grounded by ceramic mortars, passed through 200 mesh nylon sieves and stored in 4 °C for further analyses.

2.2. Analytical methods

2.2.1. THg analyses in sediments

The THg concentration in sediments was quantified using a Direct Mercury Analyzer (DMA-80, Italy) by EPA method 7473. About 0.1 g sediments were weighed and put into nickel-made sample boats, then analyzed through four modules: thermal decomposition furnace, catalytic reduction furnace, amalgamation furnace and atomic absorption furnace. For THg analyses in sediment samples, the recovery rates based on the reference material (GBW08308) ranged from 87.43% to 106.71%, the coefficient variations of replicate samples were from 7.12% to 12.33%, and the detection limit was 0.10 μg/kg.

2.2.2. Hg isotope analyses in sediments

The Hg isotope compositions were detected using a multi-collector inductively coupled plasma mass spectrometer (MC-ICP-MS) at Institute of Geochemistry, Chinese Academy of Sciences, China. In brief, about 0.5 g samples were weighed, and 5 mL aqua regia was added for digestion at 95 °C for 12 h, then BrCl was added to fully oxidize. Subsequently, 0.5 mL $NH_2OH{\cdot}HCl$ was added to remove the residual BrCl in the digests. After that, the digests were diluted with deionized water to 0.5 ng/mL THg in acidity of 10~20% for further detection. External bracketing standard Hg (NIST 3133) and internal standard Tl (NIST 997) were adopted to correct the instrumental mass bias. The analytical conditions and instrumental parameters were reported by Feng et al. [27] and Yin et al. [26]. MDF values were obtained relative to NIST 3133, and expressed as Eq. (1):

$$\delta\ \mathrm{XXXHg}(‰) = \{(\ XXXHg/\ 198Hg)_{\mathrm{sample}} \Big/ (\ XXXHg/\ 198Hg)_{\mathrm{NIST3133}} - 1\} \times 1000 \quad (1)$$

where δ^{XXX}Hg refers to δ^{199}Hg, δ^{200}Hg, δ^{201}Hg or δ^{202}Hg. The MIF is the difference in the detected δ^{XXX}Hg and the predicted δ^{XXX}Hg values, and could be calculated by Eqs. (2)–(4):

$$\Delta^{199}\mathrm{Hg} \approx \delta^{199}\mathrm{Hg} - (\delta^{202}\mathrm{Hg} \times 0.2520) \quad (2)$$

$$\Delta^{200}\mathrm{Hg} \approx \delta^{200}\mathrm{Hg} - (\delta^{202}\mathrm{Hg} \times 0.5024) \quad (3)$$

$$\Delta^{201}\mathrm{Hg} \approx \delta^{201}\mathrm{Hg} - (\delta^{202}\mathrm{Hg} \times 0.7520) \quad (4)$$

The reproducibility of Hg isotope values in sediments was evaluated by duplicate samples in every five samples. Standard reference materials (NIST 3177 (n = 4) and GSS-5 (n = 2)) were adopted for data validation, and the specific data were presented in Table S1. The uncertainties of Hg isotope values in sediments were set as larger 2 standard deviations (2 SD) in the replicate NIST 3177 or GSS-5 samples, which were 0.08‰ and 0.06‰ for δ^{202}Hg and Δ^{199}Hg values, respectively.

2.2.3. Physicochemical property analyses in sediments

The analytical methods of pH, moisture content, contents of other elements, organic matter in sediments (SOM), mean grain diameter (MGD) and the proportions of Clay, Silt and Sand in collected sediments were described in Text S1.

2.3. MixSIAR model

The MixSIAR model is developed in R 4.0.4 and detailed in Stock et al. [37]. In MixSIAR, isotope data could be used as tracers to evaluate the proportions of the potential sources in the intermingled samples by the receptor model, and quantified by the mass conservation equation. The model is calculated as follows:

$$X_{ij} = \sum_{k=1}^{p} g_{ik}\ f_{jk} + e_{ij} \quad (5)$$

where X_{ij} represents the tracers (isotope data) of j species in i samples, p refers to the assumed numbers of potential sources, f_{jk} is the isotope data of potential source k in species j, g_{ik} is the proportion of potential source k in sample i, and e_{ij} denotes the residual error [42,43,38]. For the mixed sediments in the study area, the δ^{202}Hg and Δ^{199}Hg were set as tracers and widely adopted in Hg source apportionment. The sample sites were selected as "fixed effects", which could quantify the source contributions in each site. Source data was the Hg isotope compositions (δ^{202}Hg and Δ^{199}Hg) of potential Hg sources. As a result of one sample in each site, the "Process only" was set in the error structure. When the Markov chain Monte Carlo (MCMC) run length was selected as "long", the Gelman-Rubin diagnostic variables were all lower than 1.05 and the chains have been converged to near 1, indicating the more accurate estimation of posterior distribution. The "Uninformative" was set as α = c (1, 1, 1, 1) in specify prior.

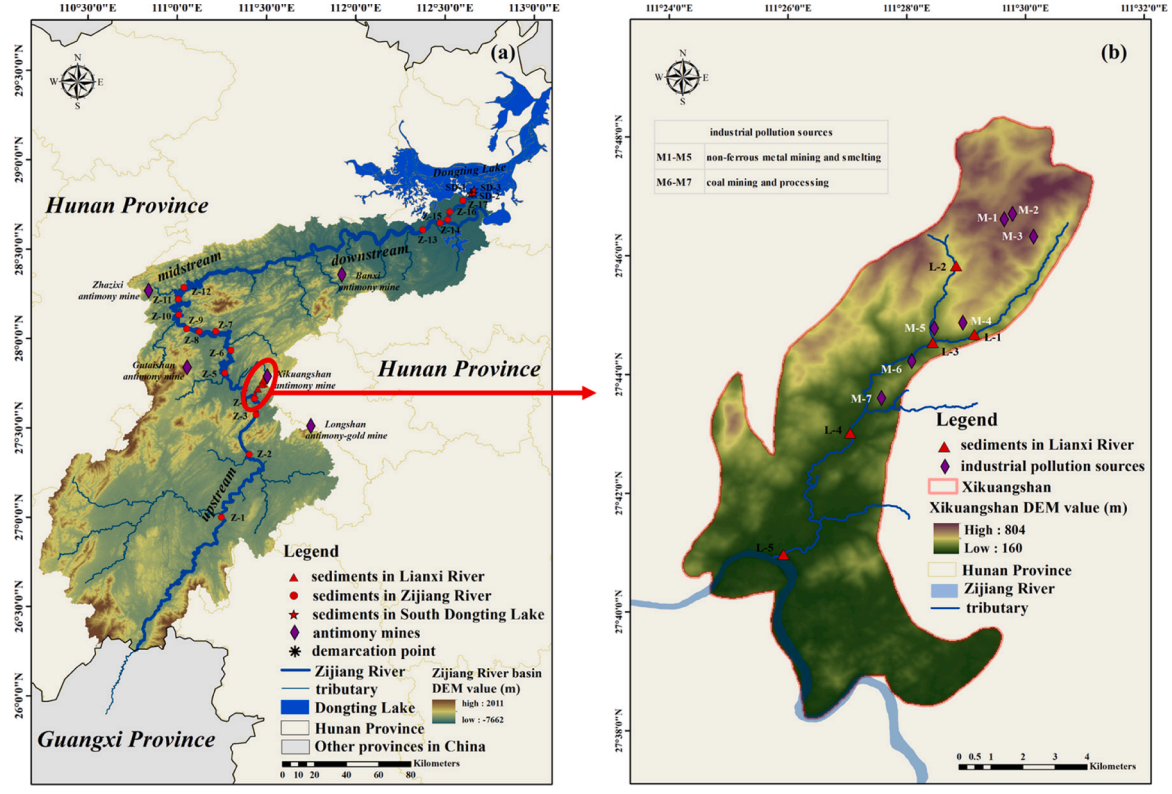

Fig. 1. The Digital Elevation Model (DEM) map of the Zijiang River basin and geographic location of sampling sites (a) and industrial activities in the Lianxi River (b).

2.4. Quality assurances and statistical analyses

Before sampling, the sediments samplers and containers were cleaned. In samples analyses, all reagents used for Hg analyses were of analytical standard. The procedural blanks were adopted to eliminate the environment interference from laboratory on Hg contents in tested samples. Satisfactory recoveries and reproducibility ensured the reliability of the analytical method and the stability of the instrument.

The spatial distribution maps of sampling points and Hg contents were performed in ArcGIS 10.2. The MixSIAR model was performed in R 4.0.4. The box diagram and histogram were generated by Origin 9.0. The statistical differences ($p < 0.05$) in sample groups were examined using ANOVA or Student's t-test in IBM SPSS Statistics 23.

3. Results and discussion

3.1. THg contents and Hg isotope values

The physicochemical properties, THg concentrations and Hg isotopic compositions of all sediments in the study area are shown in Table S2. THg concentration was used to reflect Hg pollution level and considerably ranged from 48.22 μg/kg to 4284.32 μg/kg. δ^{202}Hg varied from − 1.33–0.04‰ and Δ^{199}Hg ranged from − 0.25‰ to − 0.03‰. As shown in Fig. 2, the THg concentrations and δ^{202}Hg values of sediments in the Lianxi River (2693.78 ± 1261.14 μg/kg and −0.15 ± 0.16‰, respectively, n = 5) were significantly higher than those in the Zijiang River (249.49 ± 98.30 μg/kg and −0.72 ± 0.26‰, respectively, n = 17) ($p < 0.01$) and South Dongting Lake (113.73 ± 113.85 μg/kg and −1.08 ± 0.36‰ respectively, n = 3) ($p < 0.01$). While the Δ^{199}Hg values showed no significant difference in the above regions (−0.08 ± 0.03‰, −0.11 ± 0.06‰ and −0.16 ± 0.07‰, respectively) ($p > 0.05$). The THg concentrations in sediments were particularly high in the Lianxi River and the confluence area of the Lianxi River and Zijiang River, indicating that the riverine transport from the Lianxi River caused vital effect on Hg distribution in the Zijiang River. In addition, the THg contents and δ^{202}Hg values in the midstream (305.48 ± 78.78 μg/kg and −0.58 ± 0.23‰, respectively, n = 10) were higher than those in the upstream (241.35 ± 10.58 μg/kg and −0.94 ± 0.02‰, respectively, n = 2) and downstream (140.75 ± 47.65 μg/kg and −0.91 ± 0.18‰, respectively, n = 5), while the Δ^{199}Hg values showed no distinct spatial tendency. The average THg content in the Lianxi River was lower than that in the Dashuixi River (24285 ± 27348 μg/kg) (Table S3), where was influenced by Hg mining activities [4]. The sediments in the Zijiang River showed comparable THg concentrations with the downstream Oyapock River (278.40 ± 59.68 μg/kg), where was affected by gold mining [5]. The lower THg concentrations in the South Dongting Lake was found than that in the Moose Lake (222.93 ± 63.21 μg/kg), where was affected by gold-copper mining activities [8]. Moreover, higher δ^{202}Hg and lower Δ^{199}Hg values were observed in the Lianxi River than those in the Dashuixi River (−0.28 ± 0.35‰ and 0.10 ± 0.06‰, respectively) [4]. The sediments in the Zijiang River had higher δ^{202}Hg and Δ^{199}Hg values than those in the Oyapock River (−1.54 ± 0.22‰ and −0.40 ± 0.08‰, respectively) [5]. The sediments in the South Dongting Lake presented comparable δ^{202}Hg and Δ^{199}Hg values with those in the Luitel Lake (−1.14 ± 0.31‰ and −0.22 ± 0.22‰, respectively) [24].

In Fig. S1, the smaller MGD was observed in the downstream than that in the upstream and midstream. As shown in Fig. S2, THg in sediments significantly related with SOM ($R^2 = 0.49$, $p < 0.05$, n = 20) and Clay ($R^2 = 0.50$, $p < 0.05$, n = 20), indicating that fine particles with large amounts of organic matter played a vital role in transporting Hg, which was consistent with the result in the Bohai Sea, where the Hg contents in sediments significantly correlated with SOM and Clay [26]. Moreover, THg in sediments significantly related with Mn ($R^2 = 0.52$, $p < 0.01$, n = 20), implying Mn-(hydr) oxides strongly adsorbed Hg. The similar correlation was observed in the Eurasian Basin, where Hg distribution pattern was affected by Mn contents in sediments Kohler Stephen, Kull Laura [44]. In addition, THg concentrations in sediments had no significant relationship with pH values, moisture contents and other trace metals contents in this study area ($p > 0.05$).

3.2. Characteristics of Hg isotope compositions

The datasets of Hg isotope compositions in sediments in different aquatic ecosystems (Fig. 3a and Table S3) were compiled based on the previous reported Hg isotope ratios. The datasets were classified by the types of aquatic ecosystems (including subsidence area of mining, rivers, lakes, seas, reservoirs, estuaries and bays) and the degrees of human activities influence (industrial area, urban area, background area).

The distinct signatures of Hg isotope compositions were found in sediments affected by various Hg sources, which was consistent with the results reported by Kwon et al. [32] and Jung et al. [45]. In general, the sediments affected by industrial activities varied from − 2.02–0.64% and from − 0.88–0.19% for δ^{202}Hg and Δ^{199}Hg values, respectively. Sediments impacted by distinct industrial point sources presented varying Hg isotope characteristics. The average δ^{202}Hg values in sediments affected by metal smelting, chemical production, mining and coal-fired power were 0.06 ± 0.18‰ [4,46], − 0.39 ± 0.21‰ [29,22,28], − 0.60 ± 0.18‰ [4,30] and − 1.80 ± 0.09‰ [27], respectively. The sediments affected by coal-fired power plants showed more negative δ^{202}Hg values than those affected by other industrial point sources compiled in this study. It was attributed that sulfide removal in coal

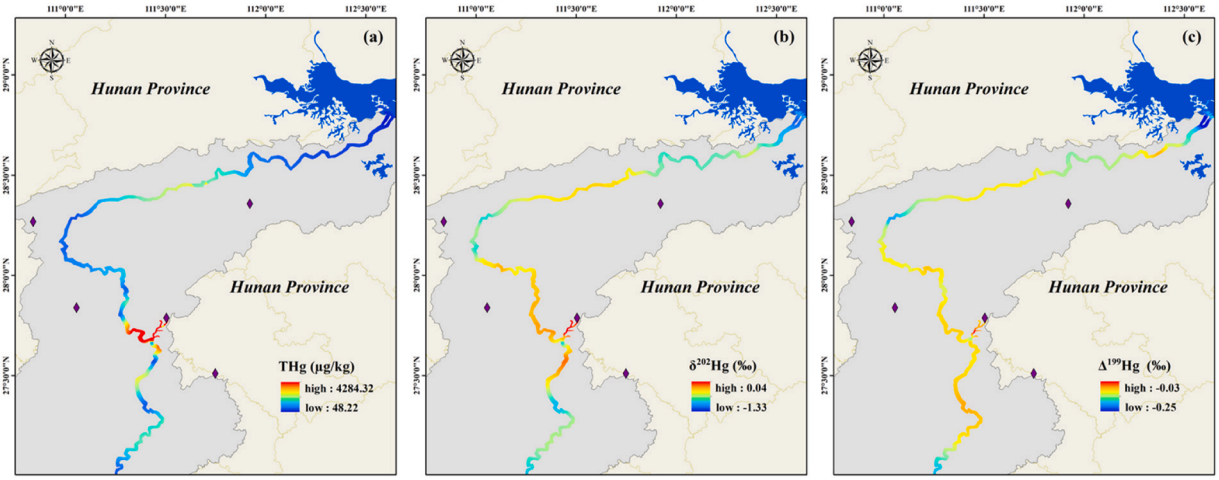

Fig. 2. Spatial distribution of THg (a), δ^{202}Hg (b) and Δ^{199}Hg (c) in sediments in the study area.

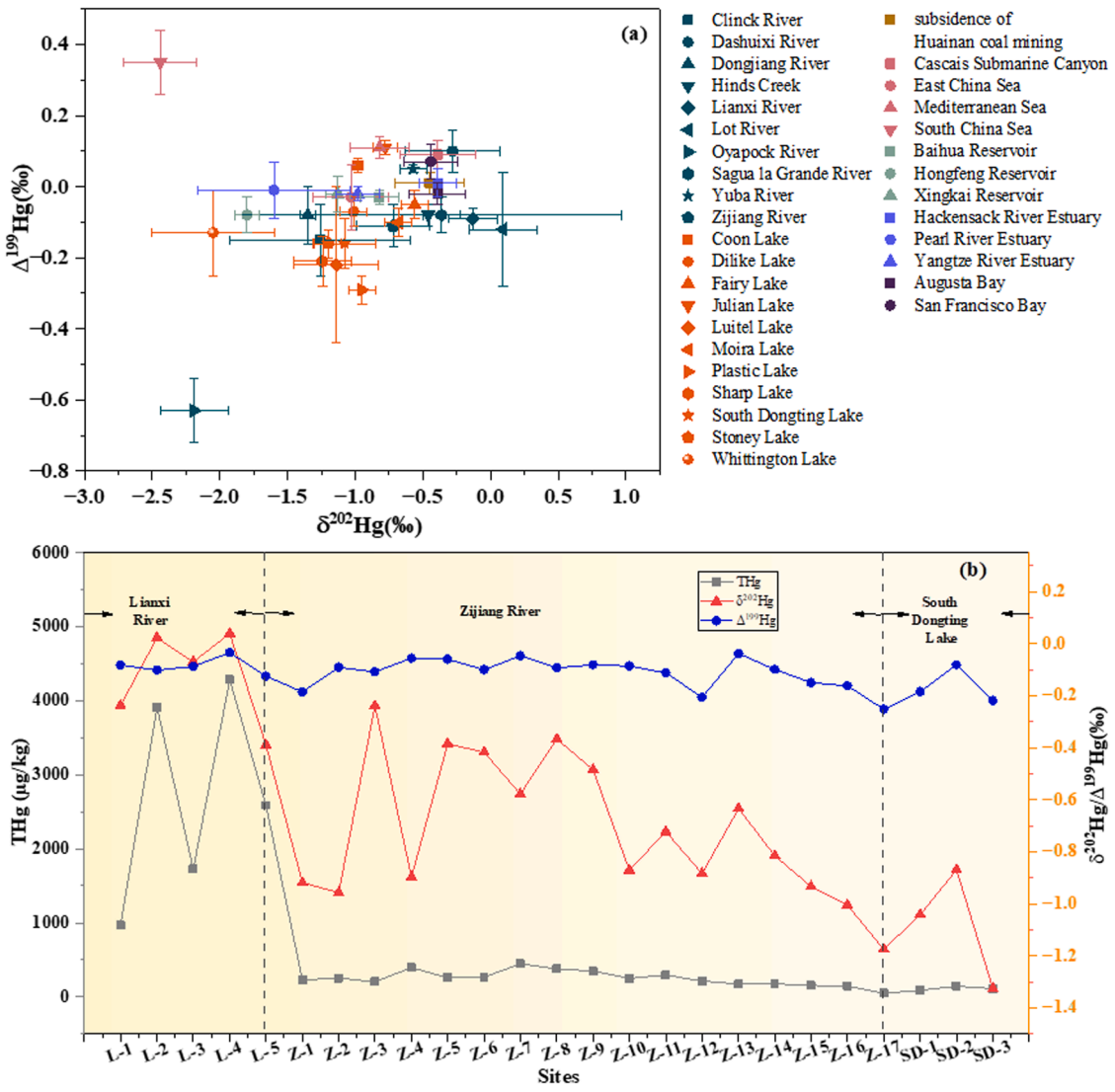

Fig. 3. Hg isotope compositions in sediments in typical aquatic ecosystems (a) and THg contents and Hg isotope compositions in sediments in the study area (b).

crushing and cleaning resulted in loss of heavier δ^{202}Hg values, further caused remaining lighter δ^{202}Hg values. Moreover, the enrichment of lighter Hg isotopes was observed in fly ash produced during combustion compared with feed coal [47]. In addition, in sediments polluted by above industrial point sources, the near-zero Δ^{199}Hg values varied in a narrow range (−0.07 ± 0.07‰, n = 234). The sediments not be affected by industrial point source showed negative δ^{202}Hg values (−1.53 ± 0.53‰) and near-zero Δ^{199}Hg values (−0.07 ± 0.11‰, n = 125) [23, 13,26], which was mainly influenced by indirect industrial transportation and urban discharges. The offshore sediments away from the Hg-contaminated sources might be derived from geogenic processes and atmospheric deposition, and presented the negative δ^{202}Hg (−2.26 ± 0.10‰) and negative Δ^{199}Hg values (−0.66 ± 0.04‰, n = 184) [13, 15]. Large Δ^{199}Hg and Δ^{200}Hg values were found in atmosphere Hg samples [48]. Gaseous elemental Hg (Hg^0) showed negative Δ^{199}Hg and Δ^{200}Hg values, while gaseous oxide Hg (Hg^{2+}) and particulate Hg (Hg_p) showed positive Δ^{199}Hg and Δ^{200}Hg values [49]. In general, relatively higher THg, relatively heavier δ^{202}Hg and negligible Δ^{199}Hg values are key evidence for Hg pollution caused by anthropogenic activities [50,22, 51].

In Fig. 3b, high THg concentrations (964.90 ~ 4284.32 μg/kg, 2693.78 ± 1261.14 μg/kg), negative to slightly positive δ^{202}Hg values (−0.39 ~ 0.04‰, −0.13 ± 0.18‰) and negative Δ^{199}Hg values (−0.12 ~ −0.04‰, −0.09 ± 0.03‰) were observed in sediments in the Lianxi River. It was consistent with the Hg isotope signatures showed by sediments affected by industrial point sources input [22,28]. Therefore, the industrial Hg input might be the primary Hg source in the Lianxi River.

In the Zijiang River, largely varied THg concentrations (48.22 ~ 448.72 μg/kg, 249.49 ± 98.30 μg/kg), negative δ^{202}Hg values (−1.17 ~ −0.24‰, −0.72 ± 0.27‰) and negative Δ^{199}Hg values (−0.25 ~ −0.04‰, −0.11 ± 0.06‰) were found in sediments (Fig. 3b). Simultaneously, the THg contents and δ^{202}Hg values generally decreased along the riverine transportation, indicating the reduced influence of human activities in downstream of the Zijiang River. Nevertheless, the THg contents and δ^{202}Hg values in sediments in the Zijiang River was still higher than those in Hg-contaminated sediments in other aquatic ecosystems [27,52]. Such observations might be attributed to the fact that the Zijiang River was affected by densely populated cities along the river. Yin et al. [26] reported that sediments affected by urban discharges have relatively higher THg concentrations, relatively heavier δ^{202}Hg and near-zero Δ^{199}Hg values. The Hg isotope compositions of some sediment samples in the Zijiang River corresponded to Hg isotope signatures of urban Hg source in some sediment samples from the Dongjiang River [13].

In the South Dongting Lake, the collected sediments with low THg concentrations (87.29 ~ 142.71 μg/kg, 113.73 ± 22.69 μg/kg)

presented negative δ^{202}Hg values (−1.33 ~ −0.87‰, −1.08 ± 0.23‰) and negative Δ^{199}Hg values (−0.22 ~ −0.08‰, −0.16 ± 0.07‰) (Fig. 3b). The THg concentrations in sediments in the South Dongting Lake were equivalent to THg concentrations in sediments not to be polluted by industrial point source [5]. The Hg isotopic compositions of sediments in the South Dongting Lake were similar to those in the Luitel Lake in France (−1.14 ± 0.31‰ and −0.22 ± 0.22‰ for δ^{202}Hg and Δ^{199}Hg values, respectively) affected by nearby industrial sources [24]. The Hg isotopic compositions of sediments in the South Dongting Lake were higher than those in the Whittington Lake in USA (−2.05 ± 0.45‰ and −0.13 ± 0.12‰ for δ^{202}Hg and Δ^{199}Hg values, respectively) less affected by human activities [23]. The sediments in uncontaminated sites showed characteristic of integrated sources from geological activities and atmospheric deposition in terrestrial environment, and the isotope compositions presented with low δ^{202}Hg and negative Δ^{199}Hg [15,49]. Therefore, the geogenic background, atmospheric deposition and human activities contributed important proportions of Hg sources in sediments in the South Dongting Lake.

Furthermore, mixing atmospheric Hg species could be differentiated by MIF values (Δ^{199}Hg and Δ^{200}Hg) [35,53]. In this study, the Δ^{199}Hg and Δ^{200}Hg values in sediments ranged from − 0.25 ~ − 0.03‰ and − 0.04 ~ 0.06‰. Thus, mixing species of gaseous elemental Hg, gaseous oxidized Hg and particulate Hg might jointly contribute to atmospheric Hg species in the basin, which was consistent with the results in Pearl River Estuary [26].

3.3. Hg sources apportionment in the Zijiang River basin

Based on the distinct Hg isotope characteristics in mixed sediments in the study area and consistent signatures with the Hg sources in sediments from the reported studies, the potential Hg sources were carefully divided into: 1) industrial Hg source from industrial activities; 2) urban Hg source from urban discharges; 3) atmospheric Hg source from atmospheric deposition and 4) background Hg source from geological processes. Source data in this study were input in the BSIMM as the form of Hg isotope compositions (δ^{202}Hg and Δ^{199}Hg) from distinct Hg sources. The end-members of Hg sources were calculated as source mean ± discrimination uncertainty (± 1 SD) in the model.

Previous studies reported δ^{202}Hg and Δ^{199}Hg isotope values of Hg-contaminated sediments were affected by metal smelting and mining activities (Table S3), including subsidence area of coal mining [54], Dashuixi River at the downstream of the ore roasting in the Wanshan Hg mining area [4], Rion Mort River affected by zinc refineries [46], Yuba River and San Francisco Bay affected by historical gold mining activities [30]. These sediments considerably affected by metal smelting and mining activities showed negative δ^{202}Hg and insignificant Δ^{199}Hg values. The end-members of δ^{202}Hg and Δ^{199}Hg values (δ^{202}Hg: −0.24 ± 0.35‰, Δ^{199}Hg: −0.01 ± 0.13‰, n = 81) from industrial Hg source in this study were estimated by the reported Hg isotope compositions in sediments affected by metal smelting and mining activities.

Vehicle exhaust emissions, waste incineration and domestic sewage discharges are important Hg sources from urban activities. Liu et al. [13] reported the Hg isotope signatures in sediments affected by urban discharges in the Dongguan city, which was consistent with the isotope compositions in the Pear River Estuary sediments affected by domestic wastewater [26]. These sediments from urban Hg source showed relatively lower MDF and insignificant MIF values. The δ^{202}Hg and Δ^{199}Hg values of urban Hg source in the BSIMM were determined as − 2.06 ± 0.25‰ and − 0.09 ± 0.01‰ (n = 24), respectively.

The background Hg isotope compositions from geogenic activities have been reported in the uncontaminated sediments in the Dongjiang River [13], Oyapock River [5], Clinch River [15]. The similar Hg isotope compositions were presented in sediments in these uncontaminated areas (Table S3). Thus, the δ^{202}Hg and Δ^{199}Hg values were considered as − 2.27 ± 0.10‰ and − 0.66 ± 0.04‰ (n = 67) for the background Hg source in the BSIMM, respectively.

Previous studies reported the large ranges of δ^{202}Hg values of atmospheric samples [49,53]. The low value of δ^{202}Hg was the significant characteristic of atmospheric Hg caused by human activities [35]. The Δ^{199}Hg values varied with Hg species in the atmosphere deposition [55]. Based on the reported Hg isotope compositions from atmospheric source in the South China Sea [26,34], Cascais Submarine Canyon (Margin [56], Mediterranean Sea [57] and San Francisco Bay [30] (Table S3), the δ^{202}Hg and Δ^{199}Hg values were found as − 1.10 ± 0.78‰ and 0.13 ± 0.15‰ (n = 73) for atmospheric Hg source in the BSIMM model, respectively.

The relative contributions of various Hg sources along the Zijiang River were quantified by the BSIMM. In Fig. 4a, the Hg isotope compositions of collected sediment samples were included in the ranges of industrial Hg, atmospheric Hg, urban Hg and background Hg, so these sources formed substantial parts of Hg sources in the study area. In the mixed matrix plot (Fig. 4b), a negative relationship was observed between industrial Hg and urban Hg, which might be attributed to the low population density and less urban activities in dense industrial areas. Besides, no significant relationship ($p > 0.05$) was presented in other Hg sources, indicating the balance in these independent Hg sources could be accurately determined.

The relative contribution values of these Hg sources in all samples are shown in Table S4 and Fig. 4c. And apparent variations of relative contributions have been observed in classified regions and shown in Table S5 and Fig. S2. In the Lianxi River, the contribution values in sediments from industrial Hg, urban Hg, background Hg and atmospheric Hg were 80.48 ± 26.38%, 12.80 ± 23.14%, 4.62 ± 4.68% and 2.10 ± 5.58%, respectively. Affected by industrial activities around the Lianxi River, the dominant Hg source in sediments was from industrial discharges, and the primary industrial Hg sources were further analyzed in 3.4 section. In the Zijiang River, Hg in sediments was mainly contributed by industrial discharges (61.39 ± 26.29%), followed by urban activities (17.83 ± 18.98%), geological processes (16.90 ± 7.68%) and atmospheric deposition (3.88 ± 6.43%). Affected by the large and super-large antimony mines, industrial Hg accounted for the largest contribution in the midstream. In the downstream, the proportion of industrial Hg decreased, whereas the proportion of background Hg increased. Simultaneously, the relative proportion of urban Hg in the Zijiang River was higher than that in the Lianxi River and the South Dongting Lake. In the South Dongting Lake, the contribution values of Hg in sediments were constituted by industrial discharges (38.33 ± 22.93%), geological processes (38.30 ± 10.23%), urban activities (12.07 ± 13.50%) and atmospheric deposition (11.30 ± 6.47%). Compared with the Lianxi River and the Zijiang River, the proportions of industrial Hg significantly decreased ($p < 0.01$), while the proportions of background Hg and atmospheric Hg significantly increased ($p < 0.01$) in the lake.

3.4. Quantification of industrial Hg sources in the Lianxi River

The Lianxi River received the released Hg from non-ferrous metal smelting and coal mining and processing in the Xikuangshan. During non-ferrous metal smelting, Hg-containing wastewater is discharged into the rivers along with the mine drainage and leachate caused by tailings [5,8]. In addition, Hg in the processes of coal mining and production is mainly discharged with gangue leaching [54], transported to the river and deposited to the sediments [58,59]. The relative contributions of multiple Hg sources in sediments in the Lianxi River could be quantified by the ternary mixing model, as follows:

$$X\delta^{202}\mathrm{Hg}_{non} + Y\delta^{202}\mathrm{Hg}_{coal} + Z\delta^{202}\mathrm{Hg}_{bac} = \delta^{202}\mathrm{Hg}_{samples} \quad (6)$$

$$X\Delta^{199}\mathrm{Hg}_{non} + Y\Delta^{199}\mathrm{Hg}_{coal} + Z\Delta^{199}\mathrm{Hg}_{bac} = \Delta^{199}\mathrm{Hg}_{samples} \quad (7)$$

$$X + Y + Z = 1 \quad (8)$$

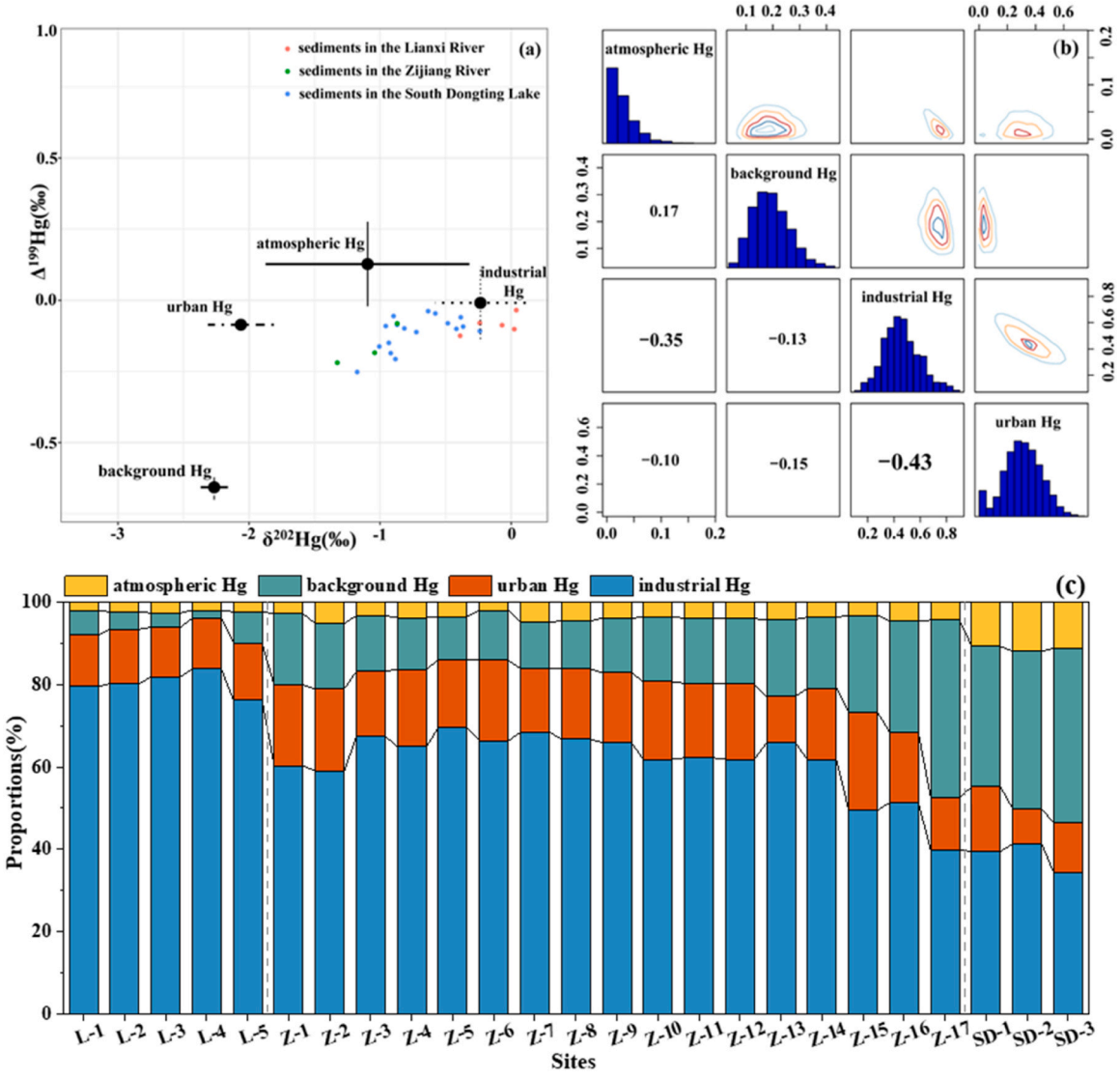

Fig. 4. Hg isotope data and source information in sediments (a), pairs plot of assumed 4 Hg sources (the value indicated the correlations between the 4 Hg sources) (b) and relative proportions of multiple Hg sources in all sediment samples (c).

where *X*, *Y* and *Z* refer to the relative contributions in the Lianxi River sediments of non-ferrous metal mining and smelting source, coal mining source and background source, respectively.

As shown in Fig. 5a, the relatively distinct Hg isotope signatures were found in sediments affected by non-ferrous metal smelting, coal mining and background process. The end-members of δ^{202}Hg and Δ^{199}Hg values of sediments in rivers contaminated by non-ferrous metal smelting source (δ^{202}Hg: 0.06 ± 0.18‰, Δ^{199}Hg: −0.07 ± 0.17‰, n = 34) were

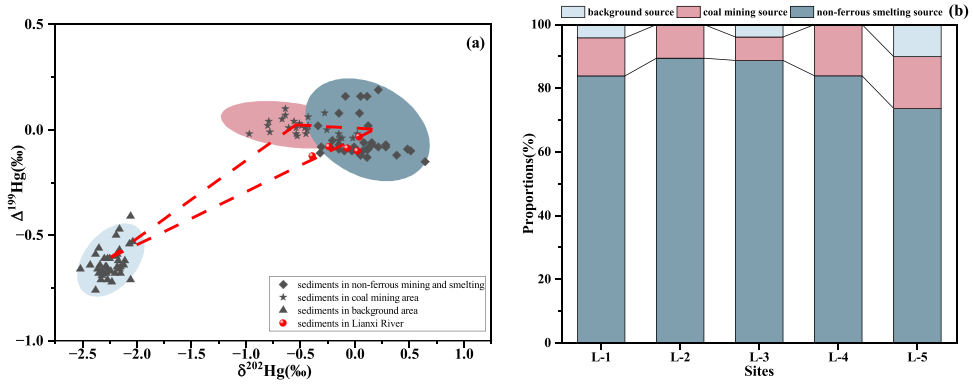

Fig. 5. Hg isotope compositions of sediments affected by non-ferrous metal mining and smelting, coal mining and background process (a) and relative contributions of multiple Hg sources in sediments in the Lianxi River (b).

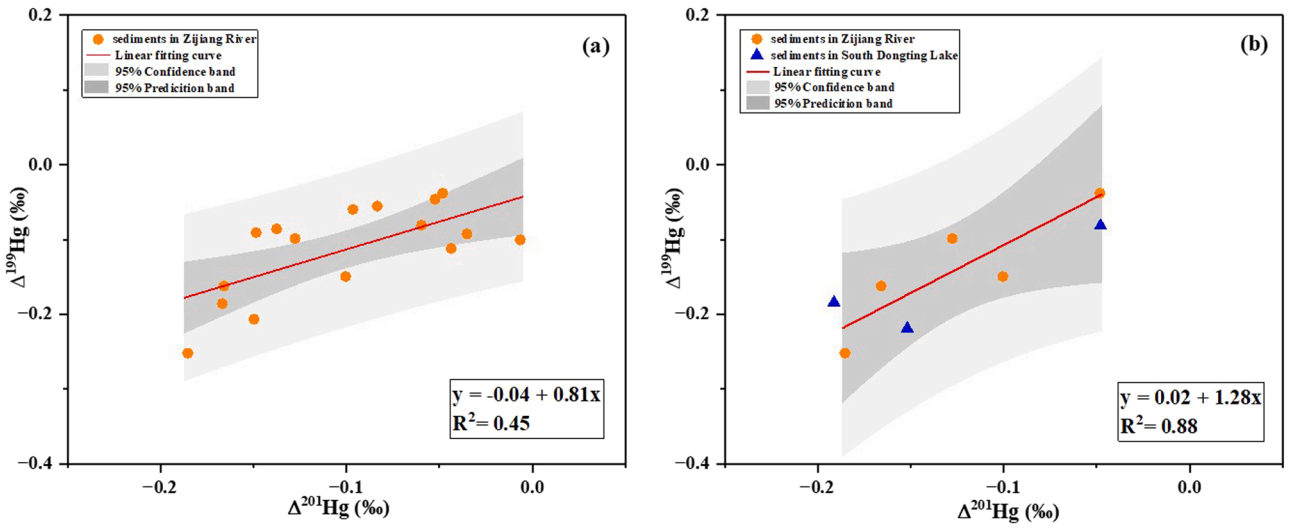

Fig. 6. Correlations between Δ^{199}Hg and Δ^{201}Hg values of sediments in the Zijiang River (a) and in downstream of the Zijiang River and South Dongting Lake (b).

estimated by sediments in the Rion Mort River around the Zn refineries areas in Lommel (Kempen, Belgium) and Viviez (Aveyron, France) [46] and sediments in the Dashuixi River affected by the Wanshan Hg mining and smelting activities [4]. The δ^{202}Hg and Δ^{199}Hg values of coal mining source (δ^{202}Hg: −0.45 ± 0.26‰, Δ^{199}Hg: 0.01 ± 0.03‰, n = 22) were determined by sediments in the subsidence area in coal mining in Huainan [54]. The end-members of δ^{202}Hg and Δ^{199}Hg values from background source (δ^{202}Hg: −2.27 ± 0.10‰, Δ^{199}Hg: −0.66 ± 0.04‰, n = 67) were set by sediments from uncontaminated upstream rivers surrounding the industrial activities [5].

As shown in Fig. 5a, the Hg isotope compositions of sediments in the Lianxi River were contained in the ranges of non-ferrous metal mining and smelting Hg origin, coal mining Hg origin and background Hg origin, indicating the vital contributions of these Hg sources in sediments in the Lianxi River. Furthermore, the relative proportions of these Hg sources in the Lianxi River were quantified by the ternary mixing model in Fig. 5b. In general, non-ferrous metal mining and smelting was the major Hg source in sediments (73.68% ~ 89.42%, 83.70 ± 0.06%), coal mining had no prominent impact in Hg pollution (7.37% ~ 16.83%, 12.59 ± 0.04%) and background process accounted for less proportions in THg contents in sediments (0.02% ~ 10.10%, 3.71 ± 4.07%) in the Lianxi River. Compared with other sites (L1, L2, L3 and L4) in the Lianxi River, the contribution of non-ferrous metal mining and smelting source in L5 relatively decreased, while the contributions of background source relatively increased, which might be attributed to the dilution effect of river transportation.

3.5. *Environmental processes of Hg*

The mechanism in MIF processes of Hg can be revealed by the ratio of Δ^{199}Hg and Δ^{201}Hg. The Δ^{199}Hg/Δ^{201}Hg of 1.00 ~ 1.30 was reported in the environmental process of Hg^{2+} photoreduction [60]. As shown in Fig. 6a, the sediment samples in the Zijiang River and South Dongting Lake presented the slope of 0.81 between Δ^{199}Hg and Δ^{201}Hg, which was close to the slope presented by sediments in the Dongjiang River (0.82) [13] and Changjiang Estuary (0.95) [61]. The sediment samples with less impact by human activities in downstream of the Zijiang River and the South Dongting Lake have the slope of 1.28 between Δ^{199}Hg and Δ^{201}Hg (Fig. 6b), which was close to the slope presented by photoreduction of Hg^{2+} in the Pearl River Estuary and South China Sea (1.05) [26].

Some studies reported that the photoreduction process in aqueous Hg^{2+} resulted in releasing Hg^0 with negative MIF, while remaining residual Hg^{2+} with positive MIF in sediments [52]. However, the negative Δ^{199}Hg values in sediments were found in this study area, which was inconsistent with the positive Δ^{199}Hg values reportfig. ed by photochemical reactions in other studies [4]. It might be attributed to the incomplete process of Hg^{2+} photoreduction. Previous researches reported the photochemical cycling of Hg was significantly affected by variable exposure to sunlight [30,62]. The high suspended solids contents (46.7 mg/L) (Mao et al., 2023) and lower water transparency of the Zijiang River might hinder the Hg^{2+} photoreduction and cause negative Δ^{199}Hg, which was consistent with the results in the Pearl River Estuary [26].

4. Conclusion

The THg contents and Hg isotope compositions in sediments were investigated to trace and quantify the relative proportions of multiple Hg sources in the study area. The spatial distribution patterns of THg and δ^{202}Hg indicated the riverine transport from the Lianxi River caused significant effects on Hg distribution in the Zijiang River. Large variations of THg and δ^{202}Hg values indicated the multiple Hg sources in this study. The potential Hg sources were classified based on the distinct Hg isotope characteristics in intermingled sediments in the study area and consistent signatures with the Hg sources in sediments from the reported studies. BSIMM concluded that industrial Hg accounted for the highest proportion in sediments in the study area, and the ternary mixing model proved the industrial Hg was dominated by non-ferrous mining and smelting in the Xikuangshan. In comparison, the contribution of industrial Hg decreased, while the contributions of urban Hg and background Hg relatively increased in the Zijiang River. Moreover, the proportion of industrial Hg significantly decreased, while the proportions of background Hg and atmospheric Hg significantly increased in the South Dongting Lake. Nevertheless, industrial Hg was the primary source in the study area, and the contributions from industrial activities deserved more attention. MIF characteristics of sediments showed the environmental processes of Hg were related to Hg^{2+} photoreduction in the Zijiang River.

Environmental implication

Mercury (Hg), a highly toxic metal, has been considered as one of the most concerned chemicals by the World Health Organization. Hg enters the environments through natural releases and anthropogenic discharges. Non-ferrous melting is one of the dominant anthropogenic Hg sources in the environment. Zijiang River basin has abundant mineral resources, prosperous industries and populated cities, resulting in

potential ecological Hg risk. This study characterized the Hg isotope signatures in sediments and quantified the relative contributions of the multiple Hg sources by isotope compositions and mixing models, which are conducive to further control Hg pollution.

CRediT authorship contribution statement

Lulu Mao: Conceptualization, Methodology, Data curation, Investigation, Writing – original draft. **Wenbo Ren:** Conceptualization, Methodology. **Xitao Liu:** Investigation, Visualization, Funding acquisition, Writing – review & editing. **Mengchang He:** Investigation, Funding acquisition, Data curation. **Chunye Lin:** Data curation, Investigation. **Ying Zhong:** Methodology, Data curation. **Yang Tang:** Methodology, Data curation. **Wei Ouyang:** Data curation, Investigation.

Declaration of Competing Interest

The authors declare that they have no known competing financial interests or personal relationships that could have appeared to influence the work reported in this paper.

Data Availability

Data will be made available on request.

Acknowledgements

This study was supported by the National Natural Science Foundation of China (Project No. 42030706).

Appendix A. Supporting information

Supplementary data associated with this article can be found in the online version at doi:10.1016/j.jhazmat.2023.132166.

References

[1] Selin, N.E., 2010. Global biogeochemical cycling of mercury: a review. Annu Rev Env Resour 34 (1), 43–63. https://doi.org/10.1146/annurev.environ.051308.084314.
[2] German, C.R., Casciotti, K.A., Dutay, J.C., Heimburger, L.E., Jenkins, W.J., Measures, C.I., et al., 2016. Hydrothermal impacts on trace element and isotope ocean biogeochemistry. Philos T R Soc A 374 (2081), 20160035. https://doi.org/10.1098/rsta.2016.0035.
[3] Kim, J., Lim, D., Jeong, D., Xu, Z., Kim, H., Kim, J., et al., 2022. Mercury (Hg) geochemistry of mid-ocean ridge sediments on the Central Indian Ridge: chemical forms and isotopic composition. Chem Geol 604, 120942. https://doi.org/10.1016/j.chemgeo.2022.120942.
[4] Yin, R.S., Feng, X.B., Wang, J.X., Li, P., Liu, J.L., Zhang, Y., et al., 2013. Mercury speciation and mercury isotope fractionation during ore roasting process and their implication to source identification of downstream sediment in the Wanshan mercury mining area, SW China. Chem Geol. 336, 72–79. https://doi.org/10.1016/j.chemgeo.2012.04.030.
[5] Goix, S., Maurice, L., Laffont, L., Rinaldo, R., Lagane, C., Chmeleff, J., et al., 2019. Quantifying the impacts of artisanal gold mining on a tropical river system using mercury isotopes. Chemosphere 219, 684–694. https://doi.org/10.1016/j.chemosphere.2018.12.036.
[6] Obrist, D., Kirk, J.L., Zhang, L., Sunderland, E.M., Jiskra, M., Selin, N.E., 2018. A review of global environmental mercury processes in response to human and natural perturbations: changes of emissions, climate, and land use. Ambio 47 (2), 116–140. https://doi.org/10.1007/s13280-017-1004-9.
[7] Xu, X.H., Meng, B., Zhang, C., Feng, X.B., Gu, C.H., Guo, J.Y., et al., 2017. The local impact of a coal fired power plant on inorganic mercury and methyl-mercury distribution in rice (Oryza sativa L.). Environ Pollut 223, 11–18. https://doi.org/10.1016/j.envpol.2016.11.042.
[8] Jackson, T.A., Telmer, K.H., Muir, D.C.G., 2013. Mass-dependent and mass-independent variations in the isotope composition of mercury in cores from lakes polluted by a smelter: effects of smelter emissions, natural processes, and their interactions. Chem Geol 352, 27–46. https://doi.org/10.1016/j.chemgeo.2013.05.036.
[9] Li, X.Y., Chen, J., Tang, L., Wu, T.T., Fu, C.C., Li, Z.G., et al., 2021. Mercury isotope signatures of a pre-calciner cement plant in Southwest China. J Hazard Mater 401, 123384. https://doi.org/10.1016/j.jhazmal.2020.123384.
[10] Pribil, M.J., Rimondi, V., Costagliola, P., Lattanzi, P., Rutherford, D.L., 2020. Assessing mercury distribution using isotopic fractionation of mercury processes and sources adjacent and downstream of a legacy mine district in Tuscany, Italy. Appl Geochem 117, 104600. https://doi.org/10.1016/j.apgeochem.2020.104600.
[11] Sun, R.Y., Hintelmann, H., Wiklund, J.A., Evans, M.S., Muir, D., Kirk, J.L., 2022. Mercury isotope variations in lake sediment cores in response to direct mercury emissions from non-ferrous metal smelters and legacy mercury remobilization. Environ Sci Technol 56 (12), 8266–8277. https://doi.org/10.1021/acs.est.2c02692.
[12] Lian, M.S., Lin, C.Y., Li, Y., Hao, X., Wang, A.H., He, M.C., et al., 2022. Distribution, partitioning, and health risk assessment of organophosphate esters in a major tributary of middle Yangtze River using Monte Carlo simulation. Water Res 219, 118559. https://doi.org/10.1016/j.watres.2022.118559.
[13] Liu, J.L., Feng, X.B., Yin, R.S., Zhu, W., Li, Z.G., 2011. Mercury distributions and mercury isotope signatures in sediments of Dongjiang, the Pearl River Delta, China. Chem Geol 287 (1–2), 81–89. https://doi.org/10.1016/j.chemgeo.2011.06.001.
[14] Li, X.Q., Pan, G.F., Zhou, A.G., Fang, L., He, N.J., 2022. Stable sulfur and oxygen isotopes of sulfate as tracers of antimony and arsenic pollution sources related to antimony mine activities in an impacted river. Appl Geochem 142, 105351. https://doi.org/10.1016/j.apgeochem.2022.105351.
[15] Donovan, P.M., Blum, J.D., Demers, J.D., Gu, B.H., Brooks, S.C., Peryam, J., 2014. Identification of multiple mercury sources to stream sediments near Oak Ridge, TN, USA. Environ Sci Technol 48 (7), 3666–3674. https://doi.org/10.1021/es4046549.
[16] Blum, J.D., Sherman, L.S., Johnson, M.W., 2014. Mercury isotopes in earth and environmental sciences. Annu Rev Earth Pl Sc 42, 249–269. https://doi.org/10.1146/annurev-earth-050212-124107.
[17] Estrade, N., Carignan, J., Sonke, J.E., Donard, O.F.X., 2009. Mercury isotope fractionation during liquid-vapor evaporation experiments. Geochim Cosmochim Ac 73 (10), 2693–2711. https://doi.org/10.1016/j.gca.2009.01.024.
[18] Rodriguez-Gonzalez, P., Epov, V.N., Bridou, R., Tessier, E., Guyoneaud, R., Monperrus, M., et al., 2009. Species-specific stable isotope fractionation of mercury during Hg(II) methylation by an anaerobic bacteria (*Desulfobulbus propionicus*) under dark conditions. Environ Sci Technol 43 (24), 9183–9188. https://doi.org/10.1021/es902206j.
[19] Zheng, W., Hintelmann, H., 2010. Nuclear field shift effect in isotope fractionation of mercury during abiotic reduction in the absence of light. J Phys Chem A 114 (12), 4238–4245. https://doi.org/10.1021/jp910353y.
[20] Zheng, W., Hintelmann, H., 2009. Mercury isotope fractionation during photoreduction in natural water is controlled by its Hg/DOC ratio. Geochim Cosmochim Ac 73 (22), 6704–6715. https://doi.org/10.1016/j.gca.2009.08.016.
[21] Bergquist, B.A., Blum, J.D., 2007. Mass-dependent and-independent fractionation of Hg isotopes by photoreduction in aquatic systems. Science 318 (5849), 417–420. https://doi.org/10.1126/science.1148050.
[22] Feng, C.Y., Pedrero, Z., Lima, L., Olivares, S., de la Rosa, D., Berail, S., et al., 2019. Assessment of Hg contamination by a Chlor-Alkali Plant in riverine and coastal sites combining Hg speciation and isotopic signature (Sagua la Grande River, Cuba.) J Hazard Mater 371, 558–565. https://doi.org/10.1016/j.jhazmat.2019.02.092.
[23] Gray, J.E., Van Metre, P.C., Pribil, M.J., Horowitz, A.J., 2015. Tracing historical trends of Hg in the Mississippi River using Hg concentrations and Hg isotopic compositions in a lake sediment core, Lake Whittington, Mississippi, USA. Chem Geol 395, 80–87. https://doi.org/10.1016/j.chemgeo.2014.12.00.
[24] Guedron, S., Amouroux, D., Sabatier, P., Desplanquee, C., Develle, A.L., Barre, J., et al., 2016. A hundred year record of industrial and urban development in French Alps combining Hg accumulation rates and isotope composition in sediment archives from Lake Luitel. Chem Geol 431, 10–19. https://doi.org/10.1016/j.chemgeo.2016.03.016.
[25] Sun, X., Yin, R.S., Hu, L.M., Guo, Z.G., Hurley, J.P., Lepak, R.F., et al., 2020. Isotopic tracing of mercury sources in estuarine-inner shelf sediments of the East China Sea. Environ Pollut 262, 114356. https://doi.org/10.1016/j.envpol.2020.114356.
[26] Yin, R.S., Feng, X.B., Chen, B.W., Zhang, J.J., Wang, W.X., Li, X.D., 2015. Identifying the sources and processes of mercury in subtropical estuarine and ocean sediments using Hg isotopic composition. Environ Sci Technol 49 (3), 1347–1355. https://doi.org/10.1021/es504070y.
[27] Feng, X.B., Foucher, D., Hintelmann, H., Yan, H.Y., He, T.R., Qiu, G.L., 2010. Tracing mercury contamination sources in sediments using mercury isotope compositions. Environ Sci Technol 44 (9), 3363–3368. https://doi.org/10.1021/es9039488.
[28] Reinfelder, J.R., Janssen, S.E., 2019. Tracking legacy mercury in the Hackensack River estuary using mercury stable isotopes. J Hazard Mater 375, 121–129. https://doi.org/10.1016/j.jhazmat.2019.04.074.
[29] Bonsignore, M., Tamburrino, S., Oliveri, E., Marchetti, A., Durante, C., Berni, A., et al., 2015. Tracing mercury pathways in Augusta Bay (southern Italy) by total concentration and isotope determination. Environ Pollut 205, 178–185. https://doi.org/10.1016/j.envpol.2015.05.033.
[30] Donovan, P.M., Blum, J.D., Yee, D., Gehrke, G.E., Singer, M.B., 2013. An isotopic record of mercury in San Francisco Bay sediment. Chem Geol 349, 87–98. https://doi.org/10.1016/j.chemgeo.2013.04.017.
[31] Lee, J.H., Kwon, S.Y., Yin, R.S., Motta, L.C., Kurz, A.Ym, Nam, S.I., 2021. Spatiotemporal characterization of mercury isotope baselines and anthropogenic influences in lake sediment cores. Glob Biogeochem Cy 35 (10). https://doi.org/10.1029/2020GB006904.
[32] Kwon, S.Y., Blum, J.D., Yin, R., Tsui, M.T.K., Yang, Y.H., Choi, J.W., 2020. Mercury stable isotopes for monitoring the effectiveness of the Minamata Convention on Mercury. Earth-Sci Rev 203, 103111. https://doi.org/10.1016/j.earscirev.2020.103111.

[33] Ma, J., Hintelmann, H., Kirk, J.L., Muir, D.C.G., 2013. Mercury concentrations and mercury isotope composition in lake sediment cores from the vicinity of a metal smelting facility in Flin Flon, Manitoba. Chem Geol 336, 96–102. https://doi.org/10.1016/j.chemgeo.2012.10.037.
[34] Meng, M., Sun, R.Y., Liu, H.W., Yu, B., Yin, Y.G., Hu, L.G., et al., 2019. An integrated model for input and migration of mercury in chinese coastal sediments. Environ Sci Technol 53 (5), 2460–2471. https://doi.org/10.1021/acs.est.8b06329.
[35] Song, Z.C., Wang, C., Ding, L., Chen, M., Hu, Y.X., Li, P., et al., 2021. Soil mercury pollution caused by typical anthropogenic sources in China: Evidence from stable mercury isotope measurement and receptor model analysis. J Clean Prod 288, 125687. https://doi.org/10.1016/j.jclepro.2020.125687.
[36] Moon, S., Huh, Y., Qin, J.H., van Pho, N., 2007. Chemical weathering in the Hong (Red) River basin: rates of silicate weathering and their controlling factors. Geochim Cosmochim Ac 71 (6), 1411–1430. https://doi.org/10.1016/j.gca.2006.12.004.
[37] Stock, B.C., Jackson, A.L., Ward, E.J., Parnell, A.C., Phillips, D.L., Semmens, B.X., 2018. Analyzing mixing systems using a new generation of Bayesian tracer mixing models. Peerj 6, e5096. https://doi.org/10.7717/peerj.5096.
[38] Stock, B.C., Semmens, B.X., 2016. Unifying error structures in commonly used biotracer mixing models. Ecology 97 (10), 2562–2569. https://doi.org/10.1002/ecy.1517.
[39] Wang, Y.N., Li, Y.R., Yang, S.Y., Liu, J., Zheng, W., Xu, J.M., et al., 2022. Source apportionment of soil heavy metals: a new quantitative framework coupling receptor model and stable isotopic ratios. Environ Pollut 314, 120291. https://doi.org/10.1016/j.envpol.2022.120291.
[40] Liu, J.K., Han, G.L., 2021. Tracing riverine particulate black carbon sources in Xijiang River basin: insight from stable isotopic composition and Bayesian mixing model. Water Res 194, 116932. https://doi.org/10.1016/j.watres.2021.116932.
[41] He, S., Li, P.Y., Su, F.M., Wang, D., Ren, X.F., 2022. Identification and apportionment of shallow groundwater nitrate pollution in Weining Plain, northwest China, using hydrochemical indices, nitrate stable isotopes, and the new Bayesian stable isotope mixing model (MixSIAR. Environ Pollut 298, 118852. https://doi.org/10.1016/j.envpol.2022.118852.
[42] Liu, M.D., Zhang, Q.R., Maavara, T., Liu, S.D., Wang, X.J., Raymond, P.A., 2021. Rivers as the largest source of mercury to coastal oceans worldwide. Nat Geosci 14 (9), 672. https://doi.org/10.1038/s41561-021-00793-2.
[43] Parnell, A.C., Inger, R., Bearhop, S., Jackson, A.L., 2010. Source partitioning using stable isotopes: Coping with too much variation. Plos One 5 (3), e9672. https://doi.org/10.1371/journal.pone.0009672.
[44] Kohler Stephen G., Kull Laura M., Heimburger-Boavida Lars-Eric, Ricardo de Freitas Thaise, Sanchez Nicolas, Ndungu Kuria, Ardelan Murat V., 2022. Distribution pattern of mercury in northern Barents Sea and Eurasian Basin surface sediment. Mar. Pollut. Bull. 185 (A), 114272. https://doi.org/10.1016/j.marpolbul.2022.114272.
[45] Jung, S., Kwon, S.Y., Hong, Y., Yin, R.S., Motta, L.C., 2021. Isotope investigation of mercury sources in a creek impacted by multiple anthropogenic activities. Chemosphere 282, 130947. https://doi.org/10.1016/j.chemosphere.2021.130947.
[46] Sonke, J.E., Schafer, J., Chmeleff, J., Audry, S., Blanc, G., Dupre, B., 2010. Sedimentary mercury stable isotope records of atmospheric and riverine pollution from two major European heavy metal refineries. Chem Geol 279 (3–4), 90–100. https://doi.org/10.1016/j.chemgeo.2010.09.017.
[47] Sun, R.Y., Heimburger, L.E., Sonke, J.E., Liu, G.J., Amouroux, D., Berail, S., 2013. Mercury stable isotope fractionation in six utility boilers of two large coal-fired power plants. Chem Geol 336, 103–111. https://doi.org/10.1016/j.chemgeo.2012.10.055.
[48] Gratz, L.E., Keeler, G.J., Blum, J.D., Sherman, L.S., 2010. Isotopic composition and fractionation of mercury in great lakes precipitation and ambient air. Environ Sci Technol 44 (20), 7764–7770. https://doi.org/10.1021/es100383w.
[49] Demers, J.D., Blum, J.D., Zak, D.R., 2013. Mercury isotopes in a forested ecosystem: implications for air-surface exchange dynamics and the global mercury cycle. Glob Biogeochem Cy 27 (1), 222–238. https://doi.org/10.1002/gbc.20021.
[50] Donovan, P.M., Blum, J.D., Singer, M.B., Marvin-DiPasquale, M., Tsui, M.T.K., 2016. Isotopic composition of inorganic mercury and methylmercury downstream of a historical gold mining region. Environ Sci Technol 50 (4), 1691–1702. https://doi.org/10.1021/acs.est.5b04413.
[51] Wiederhold, J.G., Skyllberg, U., Drott, A., Jiskra, M., Jonsson, S., Bjorn, E., et al., 2015. Mercury isotope signatures in contaminated sediments as a tracer for local industrial pollution sources. Environ Sci Technol 49 (1), 177–185. https://doi.org/10.1021/es5044358.
[52] Chen, J.B., Hintelmann, H., Zheng, W., Feng, X.B., Cai, H.M., Wang, Z.H., et al., 2016. Isotopic evidence for distinct sources of mercury in lake waters and sediments. Chem Geol 426, 33–44. https://doi.org/10.1016/j.chemgeo.2016.01.030.
[53] Chen, J.B., Hintelmann, H., Feng, X.B., Dimock, B., 2012. Unusual fractionation of both odd and even mercury isotopes in precipitation from Peterborough, ON, Canada. Geochim Cosmochim Ac 90, 33–46. https://doi.org/10.1016/j.gca.2012.05.005.
[54] Chen, X., Zheng, L.G., Sun, R.Y., Liu, S.K., Li, C., Chen, Y.C., et al., 2022. Mercury in sediment reflecting the intensive coal mining activities: evidence from stable mercury isotopes and Bayesian mixing model analysis. Ecotoxicol Environ Saf 234, 113392. https://doi.org/10.1016/j.ecoenv.2022.113392.
[55] Rolison, J.M., Landing, W.M., Luke, W., Cohen, M., Salters, V.J.M., 2013. Isotopic composition of species-specific atmospheric Hg in a coastal environment. Chem Geol 336, 37–49. https://doi.org/10.1016/j.chemgeo.2012.10.007.
[56] Mil-Homens, M., Blum, J.D., Canario, J., Caetano, M., Costa, A.M., Lebreiro, S.M., et al., 2013. Tracing anthropogenic Hg and Pb input using stable Hg and Pb isotope ratios in sediments of the central Portuguese Margin. Chem Geol 336, 62–71. https://doi.org/10.1016/j.chemgeo.2012.02.018.
[57] Gehrke, G.E., Blum, J.D., Meyers, P.A., 2009. The geochemical behavior and isotopic composition of Hg in a mid-Pleistocene western Mediterranean sapropel. Geochim Cosmochim Ac 73 (6), 1651–1665. https://doi.org/10.1016/j.gca.2008.12.012.
[58] Frossard, A., Donhauser, J., Mestrot, A., Gygax, S., Baath, E., Frey, B., 2018. Long- and short-term effects of mercury pollution on the soil microbiome. Soil Boil Biochem 120, 191–199. https://doi.org/10.1016/j.soilbio.2018.01.028.
[59] Yu, C.H., Xu, Y.P., Yan, Y.Y., Xiao, W.J., Liu, M.D., Cheng, M.H., et al., 2021. Mercury and methylmercury in China's lake sediments and first estimation of mercury burial fluxes. Sci Total Environ 770, 145338. https://doi.org/10.1016/j.scitotenv.2021.145338.
[60] Zhang, R., Russell, J., Xiao, X., Zhang, F., Li, T.G., Liu, Z.Y., et al., 2018. Historical records, distributions and sources of mercury and zinc in sediments of East China sea: implication from stable isotopic compositions. Chemosphere 205, 698–708. https://doi.org/10.1016/j.chemosphere.2018.04.100.
[61] Cheng, Y.X., Zhang, R., Li, T.G., Zhang, F., Russell, J., Guan, M.L., et al., 2019. Spatial distributions and sources of heavy metals in sediments of the Changjiang Estuary and its adjacent coastal areas based on mercury, lead and strontium isotopic compositions. Catena 174, 154–163. https://doi.org/10.1016/j.catena.2018.10.039.
[62] Gehrke, G.E., Blum, J.D., Marvin-DiPasquale, M., 2011. Sources of mercury to San Francisco Bay surface sediment as revealed by mercury stable isotopes. Geochim Cosmochim Ac 75 (3), 691–705. https://doi.org/10.1016/j.gca.2010.11.012.